CIRRUS THERMAL INFRARED SOURCE FUNCTION FROM AIRCRAFT AND SPACEBORNE MEASUREMENTS

William D. Hart*[1], Dennis L. Hlavka[1], and Matthew McGill [2]
[1]Science Systems and Applications Inc., Lanham, MD
[2]NASA Goddard Space Flight Center/613.1, Greenbelt, MD

1. INTRODUCTION

The effect of clouds upon the terrestrial radiation balance is strongly influenced by the vertical distribution of particle density relative to the temperature profile. The thermal infrared emission by the cloud into space is a convolution of the vertical emissivity of the cloud, which is related to particle density, and the Planck black body function, which is a function of temperature only. The emission to space from a point in the cloud is modulated by the optical depth of the cloud above that point. A vertical profile of the combination of these effects is referred as the thermal source function.

In the remote sensing of clouds, much effort has been given to determining the altitude of clouds in order to deduce their thermal emission characteristics. Oxygen A-band , CO2 slicing, thermal infrared brightness temperature are some techniques that use passive measurements to get cloud boundary heights. Lidars alone give cloud boundaries and particle density without providing thermal information. Techniques have been described to combine observations from these two types of instruments to derive thermal source profiles. Simultaneous active and passive observations are therefore valuable for finding the radiative effects of clouds.

The A-train satellite suite has a nadir looking lidar, CALIOP aboard CALIPSO, and a scanning spectroradiometer, MODIS aboard AQUA. A similar pair of instruments, Cloud Physics Lidar (CPL) and MODIS Airborne Simulator (MAS) or MODIS/ASTER (MASTER), was flown on the ER-2 during the TC-4 campaign in 2007. These instruments pairs provide an opportunity to determine the thermal vertical source function. Results from these instruments are best for layers of cirrus with small optical depths.

In this presentation, we will show results of computation of the thermal source function derived from these instrument pairs. For the airborne instrumentation, case studies from flight tracks over thin cirrus will be analyzed and discussed. Case studies from the spaceborne pair will be analyzed. Repeat passes over particular locations will provide opportunity for initiating a climatology of such analysis. Nearly simultaneous airborne and spaceborne observations will allow comparisons between the two techniques to be made. These studies will provide information on the feasibility of doing such analysis on a large scale and the effectiveness of remote sensing analysis done by multiple instruments on separate platforms.

2. ALGORITHM

The analysis presented here is based on one described by Platt et al. 1998 where ground based instruments were used. LIRAD is the acronym used to identify this technique where ground based lidars and radiometers view upward to sense downwelling backscattered lidar and emitted infrared energy. Our analysis uses airborne and spaceborne instrumentation, which gives an alternative perspective in that the highest clouds are closest to the sensors. As a result, cirrus is the primary cloud type for this analysis. The cloud community has a strong

*Corresponding author address: William D. Hart, Code 613.1, NASA/GSFC, 8800 Greenbelt Rd. Greenbelt, MD 20771
Email William.D.Hart@gsfc.nasa.gov

interest in the often subtle influence cirrus clouds have on the radiative balance of the atmosphere. This downward looking technique was used in an analysis described by Spinhirne et al. (1996).

The technique employed in this study relies on the energy balance described by the equation for a single cloud layer

$$\mathbf{I_r} = \mathbf{I_B}\mathbf{T}_{lw} + \mathbf{g}\eta\mathbf{S_p}\int_{\mathbf{z_b}}^{\mathbf{z_t}} \mathbf{I_{BB}(z)}\mathbf{T}_{lw}(\mathbf{z})\beta_{\mathbf{c}}(\mathbf{z})\mathbf{dz} \quad (1)$$

where $\mathbf{I_r}$ is upwelling thermal long wave infrared radiation detected by the radiometer, $\mathbf{I_B}$ is upwelling background radiation at the bottom of the cloud, $\mathbf{T}_{lw} = \mathbf{e}^{-\mathbf{g}\tau_{sw}}$ is the long wave infrared transmission of the layer, $\mathbf{g} = \sigma_{\mathbf{lw}} / \sigma_{\mathbf{sw}}$ is the ratio of the long wave extinction coefficient to the shortwave, τ_{sw} **is** the short wave optical depth of the layer, η is a multiple scattering factor which is assume to be 1 for this analysis, S_p is the shortwave extinction to backscatter ratio determined with lidar analysis, $\mathbf{I_{BB}(z)}$ is the Planck black body radiation as a function of altitude, $\mathbf{T_{lw}(z)}$ is the long wave transmission from **z** to the top of the cloud, β_c(z) is the lidar-determined backscatter coefficient, z is the vertical coordinate, and z_b and z_t are the bottom and top altitude of the cloud layer. We define the term

$$\mathbf{F_{lw}(z)} = \mathbf{T}_{lw}(\mathbf{z})\beta_{\mathbf{c}}(\mathbf{z})\Delta\mathbf{z} \quad (2)$$

where Δz is the vertical bin depth of the lidar, as the source function. It represents, when multiplied by the constants preceding the integral, the contribution of a cloud vertical element to the total long wave energy detected by the radiometer. In the analysis, the integral is evaluated by a summation $\mathbf{F_{lw}(z)}$ through the cloud layer.

In order to compute $\mathbf{F_{lw}(z)}$ **of** a cloud layer, an estimate of $\mathbf{I_B}$, the upwelling long wave energy must be made. If homogeneous conditions are assumed beneath the cloud, an estimate of the background radiance can be made by using the upwelling radiance from a clear area. Another method is to assume a typical value of $\mathbf{g}$ and computing

$$\mathbf{I_B} = \mathbf{I_{BB}(z_m)} + (\mathbf{I_r} - \mathbf{I_{BB}(z_m)}) / \mathbf{T_{lwg}} \quad (3)$$

where $\mathbf{I_{BB}(z_m)}$ is the Planck radiance at the cloud mid-point and $\mathbf{T_{lwg}}$ is the long wave transmission of the cloud found by using $\mathbf{g}$ and the cloud short wave optical depth. The maximum $\mathbf{I_B}$ found under the cloud layer would be used for the entire layer for homogeneous conditions.

The parameter $\mathbf{g}$, the ratio of long wave extinction to short wave extinction must be determined for each profile. This parameter appears both as a factor in the integral term in equation 1 and in the computation of $\mathbf{T}_{lw}$. The technique employed for this analysis uses an iterative algorithm which the computes the energy balance of equation 1 to within a certain tolerance.

3. DATA AND RESULTS

A case study was selected from the 2007 field campaign Tropical Compostion, Cloud and Climate Coupling (TC-4) which was a NASA project based in Costa Rica. The ER-2 was based at San Jose, Costa Rica. The CPL and MAS/MASTER were installed on the ER-2. TC-4 results were chosen since the CPL's data quality was good in this campaign and MAS Level-1 and Level-2 data sets were readily available. Figure 1 shows CPL and MAS products from this segment. The prevalence of multiple cloud layers throughout the campaign limited the number a cases that could be chosen. A four minute segment was selected from

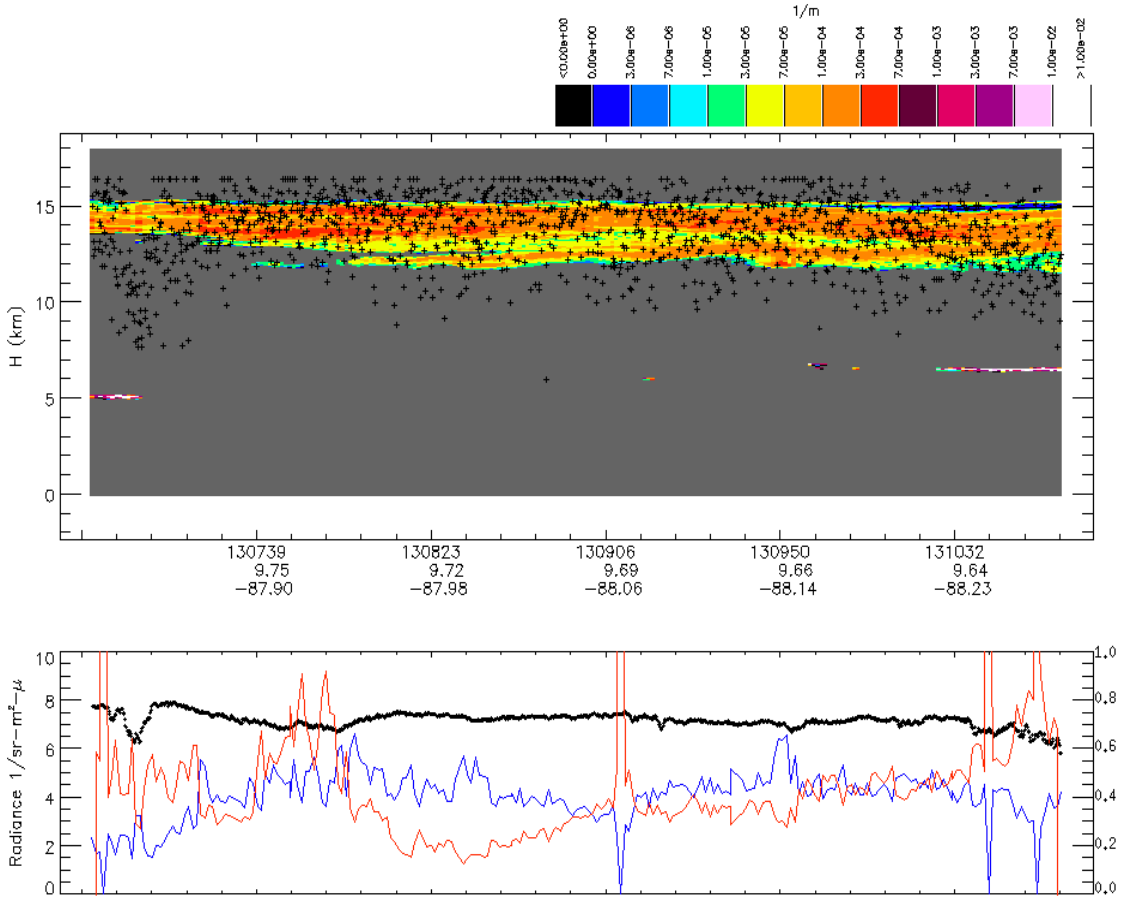

Figure 1: July 19, 2007 CPL/MAS case from TC-4. The top image shows the CPL derived extinction coefficient at 532 nm with MAS CO_2 cloud top heights superimposed in black symbols. The bottom plot shows coincident MAS long wave radiance at 10.5 μm in black along with CPL derived layer optical depth at 532 nm in blue and g in red. The right axis scale is for both optical depth and g. The axis values universal time in hhmmss format, latitude, and longitude.

19 July, 2007. This segment was chosen since it is generally a single layer of cirrus overlying the ocean.

The upper segment of Fig. 1 shows a layer of cirrus over generally clear skies with an intervening dense middle layer at the beginning and end of the segment. The CPL parameter displayed is the extinction coefficient at 532 nm. The magnitude of the extinction coefficient implies that this is a moderately dense cirrus cloud with typical midrange extinction values. The layer is transmissive to the laser for its entire length. The superimposed MAS cloud top heights, based upon CO_2 –slicing algorithm illustrate typical results of radiometer analysis of a optically thin cirrus layer. The scatter indicates that the algorithm is sensitive to other factors that are not conspicuous in the figure. An indication of the influence of lower layers on the CO_2 slicing analysis is seen where the MAS cloud tops trend toward the middle cloud at the segment's begining and end. The lower figure segment shows the MAS observed radiance at 10.5 μm which is used in the source function computation, but not in CO_2 slicing. The MAS radiance shows a decreasing trend in the single-layer left half of the plot as the CPL optical thickness, shown in blue, shows an increase. This is an expected result. The red line in the lower plot

shows the value of the ratio of long-wave extinction to the short wave extinction, $\mathbf{g}$, determined by the iterative method mentioned under equation 3. It shows an increasing value as the optical depth increases. Its range of values in the clear area from 0.25 to 0.55 is in the expected range. The values before 13:08:05 range from high to low, possibly because of multiple layer issues.

Fig. 2 shows the source function $\mathbf{F_{lw}(z)}$ given by equation 2. The black markers indicate the altitude where the maximum is for each profile. The maximum for this case tends to be in the middle region of the cloud. In the time region near 13:09:50 the maximum is near the bottom of the cloud where there is a dense cloud element. At 13:08:23, the maximum is at the top of the cloud where is a denser cloud element exists as indicated by the extinction image in Fig. 1. The level of the maximum may be considered an median center from which the long wave energy originates and influence where long wave radiometer algorithms find cloud tops. The results clearly show the advantage of combining the lidar with radiometer data to derive the vertical thermal structure of the cirrus cloud.

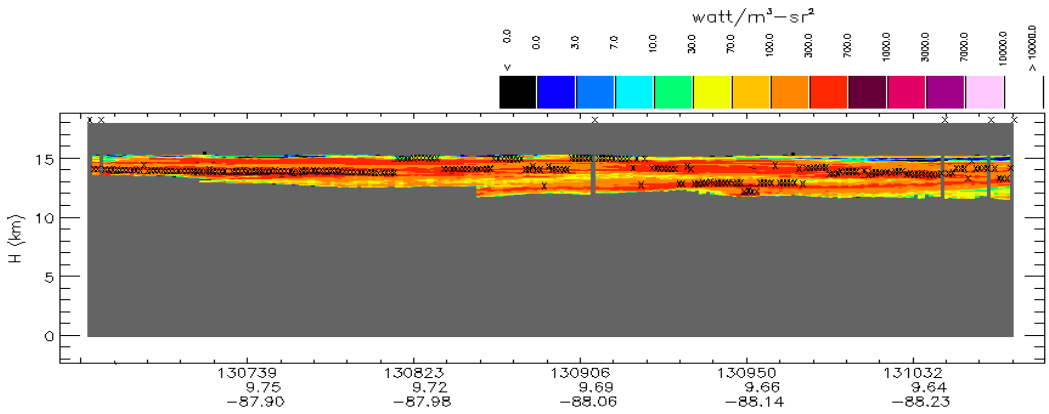

Figure 2: Thermal source function derived from CPL and MAS products for the TC-4 case study segment. The black markers indicate the level of the maximum for each profile.

4. SUMMARY AND CONCLUSIONS

This presentation provides an analysis that shows a method to determine the vertical structure of cirrus clouds using airborne and spaceborne combination of lidar and radiometer observations. A parameter termed thermal source function is used to show the structure. Equations of an algorithm are presented and results from a case study from the NASA campaign TC-4, 2007 are shown. The case demonstrates the potential for the analysis to reveal the influence that cirrus cloud have on the radiative balance at long wave infrared wavelengths. Routine use of such an algorithm in appropriate circumstances would enhance the overall measurement of the radiative effects of cirrus clouds.

At the time of submission of this abstract, analysis of similar cases from MODIS and CALIOP were still in progress. Also, additional airborne cases and possibly simultaneous airborne and spaceborne cases will be found and analyzed. These will be presented as a poster at the ICCP conference.

5. ACKNOWLEDGEMENTS

MODIS Airborne Simulator

MAS products for the case study were provided by T. Arnold of NASA/GSFC. Also see
King, Menzel, Grant, Myers, Arnold, Platnick, Gumley, Tsay, Moeller, Fitzgerald, Brown, and Osterwisch, 1996: Airborne scanning spectrometer for remote sensing of cloud, aerosol, water vapor and surface properties. Journal of Atmospheric and Oceanic Technology, 13, 777-794.

Cloud Physics Lidar

CPL data products are publicly available at http://cpl.gsfc.nasa.gov

6 REFERENCES

Platt, C.M.R., S.A. Young, P.J. Manson, G.R. Patterson, S.C. Marsden, R.T. Austin, and J.H. Churnside, 1998: The Optical Properties of Equatorial Cirrus from Observations in the ARM Pilot Radiation Observation Experiment. *J. Atmos. Sci.*, **55**, 1977–1996.

Spinhirne, J.D., W.D. Hart, and D.L. Hlavka, 1996: Cirrus Infrared Parameters and Shortwave Reflectance Relations from Observations. *J. Atmos. Sci.*, **53**, 1438–1458.